*Desalination and Water Treatment*
www.deswater.com

doi: 10.1080/19443994.2015.1042066

57 (2016) 9420–9436
April

Taylor & Francis
Taylor & Francis Group

# Adsorption of arsenic (V) ions onto cellulosic-ferric oxide system: kinetics and isotherm studies

Surabhi Sharma[a], K. Balasubramanian[a,*], Rajat Arora[b]

[a]*Department of Materials Engineering, Defence Institute of Advanced Technology (DU), Pune, India, Tel. +91 020 24304207; Fax: +91 020 24388835; emails: surabhi.gecu@gmail.com (S. Sharma), meetkbs@gmail.com (K. Balasubramanian)*
[b]*Department of Metallurgical Engineering, Indian Institute of Technology (BHU), Varanasi, India, email: rajat.arora.met12@itbhu.ac.in*

Received 17 October 2014; Accepted 7 March 2015

ABSTRACT

A novel microporous adsorbent, cross-linked cellulose acetate matrix impregnated with $Fe_2O_3$ was synthesized by precipitation method for the expunging of As (V) ions. Elimination of As (V) ions was successfully executed through adsorption from prepared arsenate solution in preliminary batch systems. Various parameters affecting adsorption of analyte ions viz. solution pH, $Fe_2O_3$ content in beads, amount of adsorbent, contact time, and initial concentration of As (V) ions were satisfactorily interpreted. Optimized adsorption percentage of 65% was recorded with initial concentration of As (V) ions as 10 $mgL^{-1}$ in the pH range of 5.0, using 1gm of adsorbent impregnated with 20 wt.% $Fe_2O_3$ in 4 h; characterization of the adsorbent was executed by X-ray diffraction, scanning electron microscopy, Fourier transform infrared, and BET theory. Langmuir, Freundlich, Temkin, and Dubinin–Radushkevich equilibrium adsorption isotherm models were studied to determine the nature and process of adsorption. Adsorption kinetics was found to be in a commendable agreement pseudo-first-order mechanism. The adsorbent was found to be efficacious up to 5 cycles of adsorption without considerable decrease in efficiency. Thermodynamic investigation established that adsorption of As (V) ions was a spontaneous process with free energy change −8.38 kJ/mol. The present prospective provides a cost-effective and efficient approach that can be used to moderate the arsenic concentration to environmental acceptable level.

*Keywords:* Arsenic (V) ions; Cellulose acetate; Ferric oxide; Adsorption; Isotherms-kinetics

## 1. Introduction

Ubiquitous and catastrophic nature of arsenic has attracted significant attention for its remediation from aqueous media as it is considered to be fatal, and its accumulation over a period of time in human bodies can be detrimental and cause astringent health hazards [1]. Major route of arsenic exposure is liable through ingestion of contaminated drinking water and being a validated carcinogen, mutagenic, and teratogenic [2], it can cause gastrointestinal damage, skin cancer, kidney cancer, cardiovascular, neurological, and endocrine disorders in the human body [3].The rising content of arsenic in drinking water is an alarming subject that demands immediate dextrous

*Corresponding author.

attention [4–6]. Stringent regulations have been made to curtail the threat to human health, for example, United States Environmental Protection Agency has lowered the drinking water contaminant limit for arsenic to 10 μg/L which was earlier 50 μg/L, effective from January 2006 [7]. The WHO has also recommended a maximum of 10 μg/L dissolved arsenic in drinking water, therefore its eradication from aqueous media is of paramount importance [5]. Arsenic occurs in natural water in its inorganic form, either in trivalent state, As (III) being of chief concern because of its greater lethality, and/or pentavalent state, As (V), with latter being thermodynamically stable and occurs in oxygenated surface waters [8–10]. Apart from its natural occurrence in earth's crust, it enters the environment and ecosystem through the industrial wastes, arsenical pesticides, and herbicides, through the dust from burning of fossil fuels and mining, especially as a by-product of copper, gold, and lead refining [1]. Several countries have reported the existence of arsenic in contaminated water, for example, in the Bengal basin area of Bangladesh and West Bengal in India, a prominent section of population is under serious peril of arsenic contamination [11,12].

Various conventional physical methods such as precipitation [13], cementation [14], electrodialysis [15], membrane technologies, ion exchange [16], and complexation with polyvalent metal [17] have been executed for removal of heavy metal ions from aqueous systems over the last two decades. Low-cost and natural adsorbents such as coffee beans, coconut coir, corn cobs, human hair, newspaper, tea leaves, sunflower seeds, wheat straw, rice hulls, and cotton seed husks have been effectively used for the removal of arsenic from water systems [5]. Alginate and carboxymethyl cellulose beads were prepared for the removal of As (V) ions [5]. Lignocelluloses substrate loaded with ferric ion has been used for adsorption of As (III) and As (V) [4]. Low-cost inorganic adsorbents such as zeolite, bentonite, sepiolite, pyrolusite, and limonite have also been utilized for selective removal of As (III) and As (V) from water [10]. Fe/Glass has also been employed as an adsorbent [18]. Fe and Al-doped micro and nanoparticles have been put to use for the elimination of fluoride and arsenic (V) ions from water [19].Cellulose beads loaded with iron oxyhydroxide has also been reported in the literatures for detoxification and reclamation of aqueous media by removal of As (III) and As (V) [20]. Some of the contemporary and polished analytical methods include the use of Carbon nanotubes [21,22] via the technique of solid phase extraction [MWCNTs], which involves high capital investment and application of Fe/Carbon aerogel structures for enhanced arsenic removal efficiency [22,23].

In this research, a novel, cost-effective and efficient adsorbent, magnetised cellulose beads tinctured with $Fe_2O_3$ was synthesized by rapid precipitation method. Supplementary advantages obtained due to loading of nano $Fe_2O_3$ particles in the cellulose matrix are: (1) Elementary and rapid separation of beads due to the magnetic behavior of cellulose acetate once the equilibrium is attained, (2) augmentation of adsorption capacity due to the presence of acetate and hydroxyl functional groups of cellulose which in turn increased the porosity of the impregnated matrix providing ample surface area for adsorption, and economical and environment compatible adsorbent [24].

To the best of our cognition, no former works have synthesized this adsorbent and used it for selective removal of As (V) ions. These beads were used as an adsorbent for expunging of As (V) ions from mimicked effluent systems the experimental results were assayed as a function of time, solution pH, initial As (V) ion concentration, amount of beads, and wt.% $Fe_2O_3$ loading in the beads. The equilibrium adsorption isotherms were examined using the Langmuir, Freundlich, Temkin, and Dubinin–Radushkevich (D–R) isotherm models. Sorption kinetics were analysed to predict the pathway and mechanism of the reaction which well fitted with pseudo-first-order, Elovich and intraparticle diffusion models. Thermodynamic investigation was carried out to understand the nature of adsorption procedure at 300 K. The repercussions of this study permit us to evaluate the pertinence of cross-linked magnetised cellulose acetate beads for removal of As (V) from aqueous solution.

## 2. Materials and methods

All chemicals used were of analytical reagent grade and were used without further treatment and purification, unless stated otherwise. Cellulose acetate, ferric oxide ($Fe_2O_3$), epichlorohydrin ($C_3H_5ClO$), sodium chloride (NaCl), sodium hydroxide (NaOH), N,N-Dimethylacetamide $CHCN(CH)_2$, acetone ($CH_3COCH_3$), sodium arsenate ($Na_2HAsO_4$), potassium iodate ($KIO_3$), azure B, and sodium acetate ($CH_3COONa$) were all procured from Merck Inc. India and used as received. Distilled deionized water was used throughout the experimental work.

### 2.1. Synthesis of impregnated magnetised cellulose beads

To synthesize impregnated cellulose beads, requisite amount of $Fe_2O_3$ was dispersed through sonication in the solvent system containing N, N-Dimethylacetamide: Acetone (1:2) for 15 min.

Further, estimated amount of cellulose acetate was added to this mixture and stirred progressively to obtain a dispersed solution. Epichlorohydrin (1 vol %) was added to this solution to develop *in situ* cross linking. NaCl was further introduced to enhance the porosity of the beads [25]. The resulting mixture was precipitated in an acid coagulation bath containing 0.1 M HCl to obtain uniform sized spherical beads [9]. The beads thus formed, were filtered from the acid coagulation bath and immersed in deionized water to remove traces of acid and leach out NaCl, resulting in formation of beads with profound porosity. The resultant beads were then, hydrolysed using 0.1 M NaOH, washed thoroughly several times with deionized water and air-dried at room temperature till constant weight. Fig. 1 depicts the synthesis of magnetised cellulose acetate beads.

### 2.2. Preparation of stock solution

Stock solution of As (V) ions was prepared by dissolving 100 mg sodium arsenate in 1,000 mL deionized water. Working standard solutions of As (V) were prepared by diluting stock solution with respective amounts.

### 2.3. Batch sorption experiments

Effect of various experimental parameters was monitored by batch adsorption studies. Variation with pH of the solution, wt.% of $Fe_2O_3$ loading in the beads, weight of the adsorbent (dose) was monitored. Also, the time dependant uptake of analyte ions from the solution was analysed maintaining optimum conditions viz. pH 5.0, 20 wt.% Fe-loaded beads with a constant volume (100 mL) of the solution containing As (V) ions of varying initial concentrations (10 mg/L, 30 mg/L, and 50 mg/L) at ambient temperature 300 K for 5 h. The conical flask containing adsorbent and adsorbate was agitated for predetermined time intervals on a mechanical shaker with 720 rpm. The supernatant solution was filtered and amount of As (V) ions was analysed using Atomic Absorption Spectrophotometer (AAS hydride vapour generator (AASHVG-1) 6300 Shimadzu). Simultaneously, the concentration of As (V) ions was also examined spectroscopically using the dye Azure B [26,27] using nanodrop UV-Visible Spectrophotometer (NANO DROP, ND-1000). The adsorption capacity ($q$) and the adsorption efficiency (% Ad) were evaluated as:

$$\%\ \mathrm{Ad} = \frac{C_0 - C_e}{C_0} \times 100 \tag{1}$$

$$q_e = \frac{C_0 - C_e}{M} \times V \tag{2}$$

where $C_0$ and $C_t$ are the initial As (V) ion concentration and As (V) ion concentration at time $t$ (mg $L^{-1}$), respectively, $w$ is the amount of the adsorbent used and $V$ is the total volume (L) of the solution.

### 2.4. Characterization

Scanning electron microscopy (SEM) was used (Jeol JSM-840 A) to scrutinize the surface morphology of cellulose acetate beads. Fourier transform infrared (FTIR) spectroscopy was carried out (Bruker$^{TM}$-380) in the wavelength range 400–4,000 $cm^{-1}$ for functional group analysis. Cellulose acetate beads were analysed by X-ray diffraction (XRD) using Bruker AXS D8 advance diffractometer with Cu Kα radiation, in the $2\theta$ ranging from 10–80˚.

### 2.5. Adsorbent reuse

Recyclability of beads was investigated by performing several cycles of adsorption and subsequent elution. It was found that the adsorbent could be used efficaciously up to five cycles without significant decrease in recovery of analyte ions.

## 3. Results and discussion

Cross-linked magnetized cellulose beads loaded with $Fe_2O_3$ with variable weight % of $Fe_2O_3$ (1, 5, 10, 15, 20, 30) were successfully synthesized by precipitation polymerization technique. Hybrid cellulose acetate beads exhibited good mechanical properties by virtue of cross linking.

### 3.1. Characterisation

Surface morphology of the beads was examined using scanning electron microscopy; the SEM micrographs of the impregnated cellulose beads confirmed the shape of the beads to be uniformly spherical with an average diameter of 1.5 mm (Fig. 2(a)). Fig. 2(a) and (b) revealed the surface morphology and reflected the presence of micropores and voids. In SEM micrographs of adsorbent loaded with As (V) ions, prominent disappearance of flow lines, voids, and micropores could be observed as depicted by Fig. 3(a) and (b). The adsorption of As (V) ions onto the as prepared adsorbent was further confirmed by three dimensional images of adsorbent loaded with As (V)

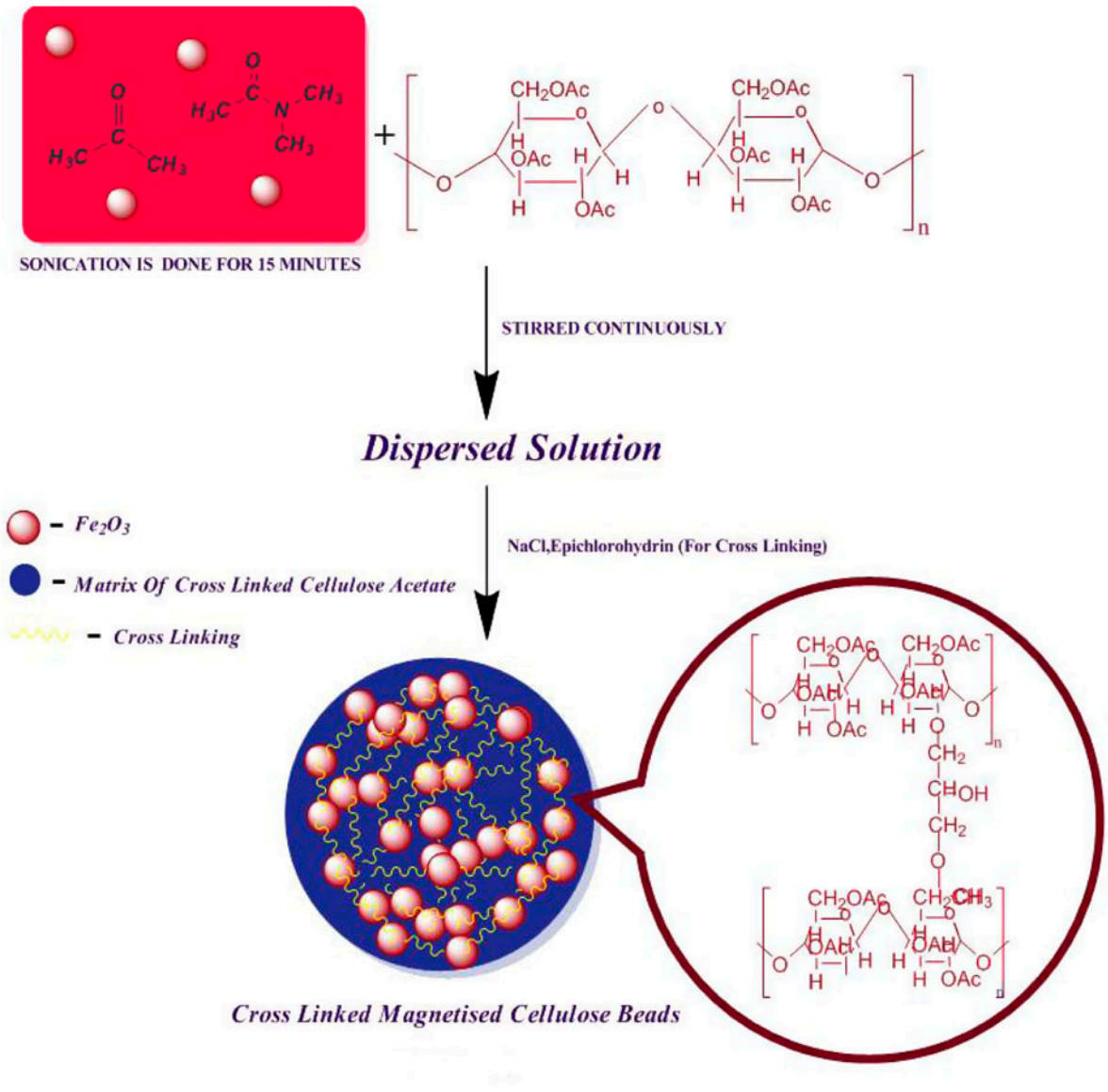


Fig. 1. Schematic describing the synthesis of magnetised cellulose acetate beads.

ion obtained by Atomic Force Microscopy (AFM) (Fig. 3(c) and (d)). XRD analysis of cellulose acetate (CA), magnetised cellulose acetate beads (CA-$Fe_2O_3$), arsenic-loaded hybrid beads (As (V)–CA-$Fe_2O_3$) are shown in Fig. 3(e). In XRD pattern of cellulose acetate, diffraction peaks appeared at $2\theta = 18.35^\circ$ and $22.09^\circ$ corresponding to amorphous nature of cellulose acetate. These values correspond to (1 0 1) and (0 1 2) lattice planes, respectively. Crystalline $Fe_2O_3$ was found to exhibit sharp peaks between 30 and 40° [28]. A wide peak in between 20 and 30° and sharp peaks in between 30 and 40° in CA-$Fe_2O_3$ beads represent the dispersion of iron oxide ($Fe_2O_3$) in integrated matrix of cellulose acetate. This diffraction pattern confirms the increment in crystalline nature of cellulose acetate, which may alter its adsorption capacity. A similar kind of pattern was observed for As (V)-loaded magnetised beads (As (V)–CA-$Fe_2O_3$) with slight variation in intensity of the peaks.

The FTIR spectra of Iron oxide ($Fe_2O_3$), cellulose acetate and impregnated cellulose acetate beads are shown in Fig. 3(f). The characteristic bands of cellulose acetate in the IR spectrum could be evidently seen. IR Bands at 1,044 $cm^{-1}$ characterize for the C–O–C (ether linkage) glycosidic units. Broad absorption band at 3,300–3,500 $cm^{-1}$ corresponds to stretching of –OH group [29,30]. The alcoholic free –OH stretching was observed at 3,763 and 3,614 $cm^{-1}$. A peak is observed

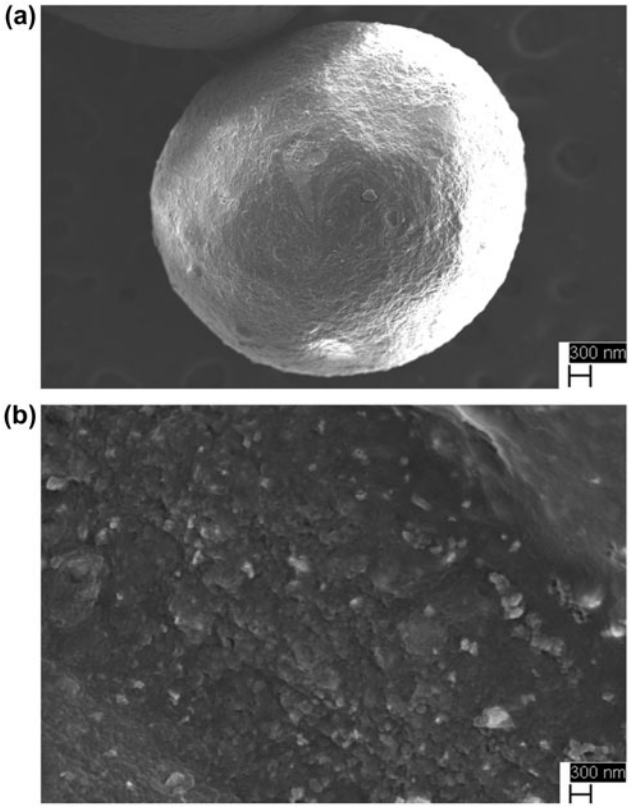


Fig. 2. (a) SEM micrograph of magnetised cellulose bead and (b) Magnified SEM image of the bead.

at 3,443 $cm^{-1}$, which corresponds to the strong interaction of –OH stretching vibration from the acetate group in cellulose acetate [31]. The curtailment in the intensity of the peak at 2360.06 $cm^{-1}$ in the spectrum of cellulose acetate, along with deviation in intensity and width of peak at 549 $cm^{-1}$ in spectrum of $Fe_2O_3$-loaded cellulose acetate beads was observed which could be due to interactions of iron oxide ($Fe_2O_3$) with cellulose acetate, the peak 549 $cm^{-1}$ is present in the CA, and same peak appears in the $Fe_2O_3$-loaded CA, there was no change in deviation and intensity was observed by the authors during experimentation. The $Fe^{2+}$ ions are expected to complex with the oxygen of the carbonyl group that has arisen from oxidization of cellulose hydroxyl group to either keto or aldehyde group [32]. The unreacted hydroxyl groups are expected to form complexes with iron involving cation exchange/ substitution reactions [33,34]. The presence of 1,516 $cm^{-1}$ peak depicts the presence of the carboxylic group present in the cellulose acetate, whose intensity is reduced due to the introduction of $Fe_2O_3$ in the matrix of beads. As observed by Sundar et.al, a cellulose molecule has three alcohol groups present, which reacts with strong acid or base, in this case, HCl and NaCl, to form $H^+$ ions, when $Fe^{2+}$ is introduced, $Fe^{2+}$ coordinates with the oxygen atoms present in these ions, thus causing the disappearance [35]. The peak in this region (1,510–1,520 $cm^{-1}$) represents the asymmetrical vibration of O=C–C=O or bidentate $Fe^{2+}$ complex such as –C–O–Fe–O–C– engaged in coordinate bond formation [32].

### 3.2. Effect of parameters affecting adsorption

#### 3.2.1. Influence of pH

Effect of pH on the sorption of analyte ions was monitored in 10 mg/L concentration of As (V) ions, adjusting pH from 3 to 8 and processed according to the suggested procedure. Adsorption increased with increasing pH and maximum adsorption of 34% was

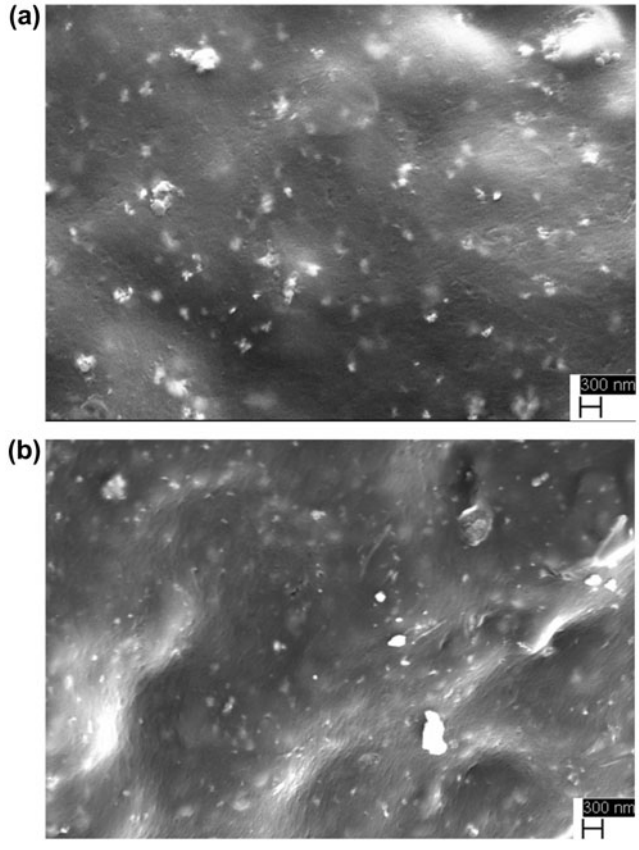


Fig. 3. (a,b) SEM images of the bead after adsorption of As (V) ions, (c,d) AFM images of the bead after adsorption of As (V) ions, (e) XRD pattern of cellulose acetate (CA), magnetised cellulose acetate beads (CA-$Fe_2O_3$), arsenic-loaded hybrid beads (As (V)-CA-$Fe_2O_3$), and (f) IR spectra of iron oxide ($Fe_2O_3$), cellulose acetate and impregnated cellulose acetate beads.

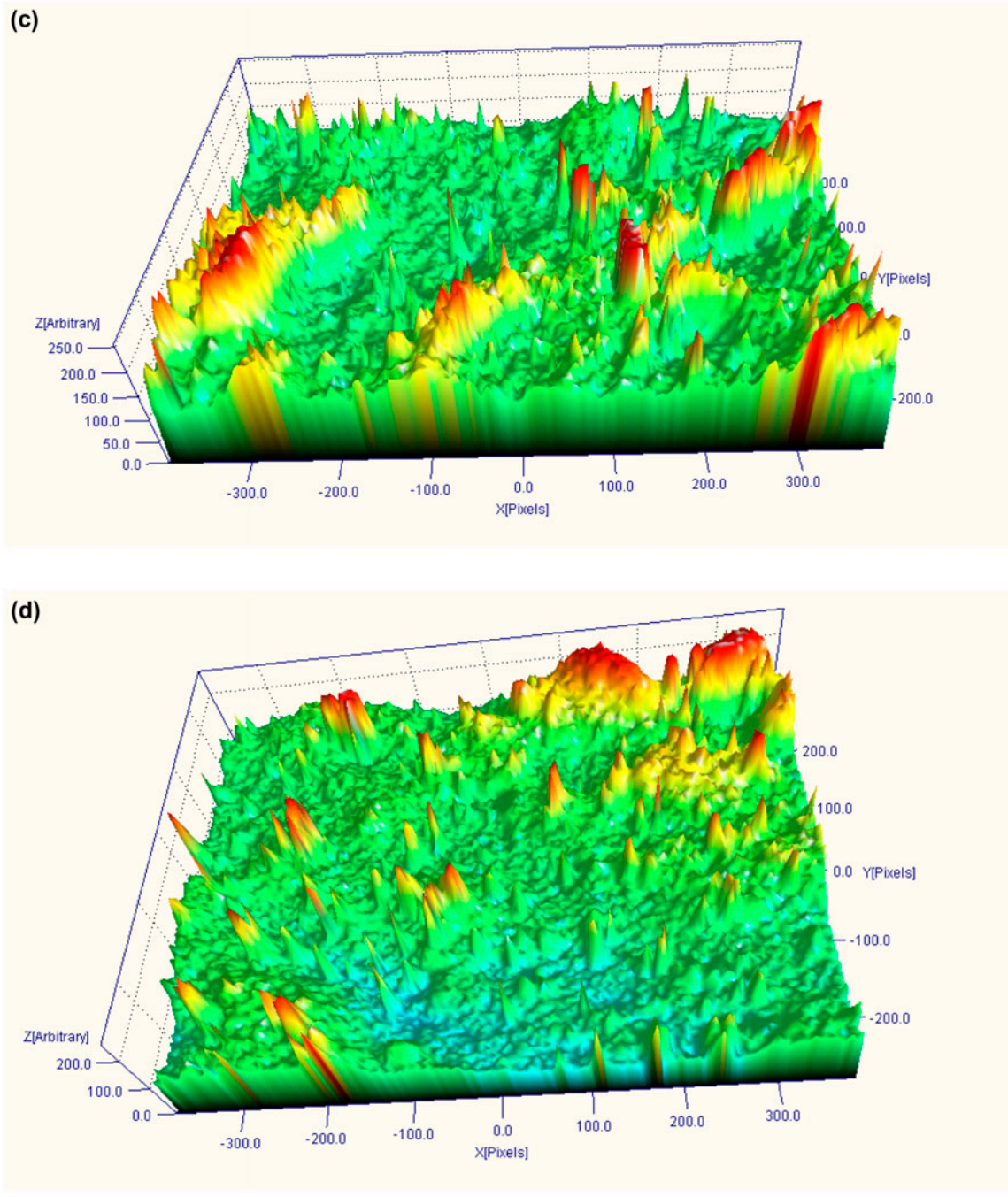


Fig. 3. (*Continued*).

recorded at pH 5.0 (Fig. 4(a)), which may be attributed to presence of optimum amount of $H^+$ ions. With further increase in pH, adsorption of As (V) ions was suppressed (Fig. 4(b)). In oxidizing conditions, $(H_2AsO_4)^-$ species dominates at lower pH values [18]. Hence, in the pH range of 3.0–6.0, the removal of As (V) ions may be represented as:

$$Fe_2O_3 + 6(H_2AsO_4)^- + 6H^+ = 2Fe(H_2AsO_4)_3 + 3H_2O \quad (3)$$

Beyond pH 6.0, the amount of $H^+$ ions present in the solution may not be sufficient and a decline in the extent of adsorption was observed. Hence, pH 5.0 was

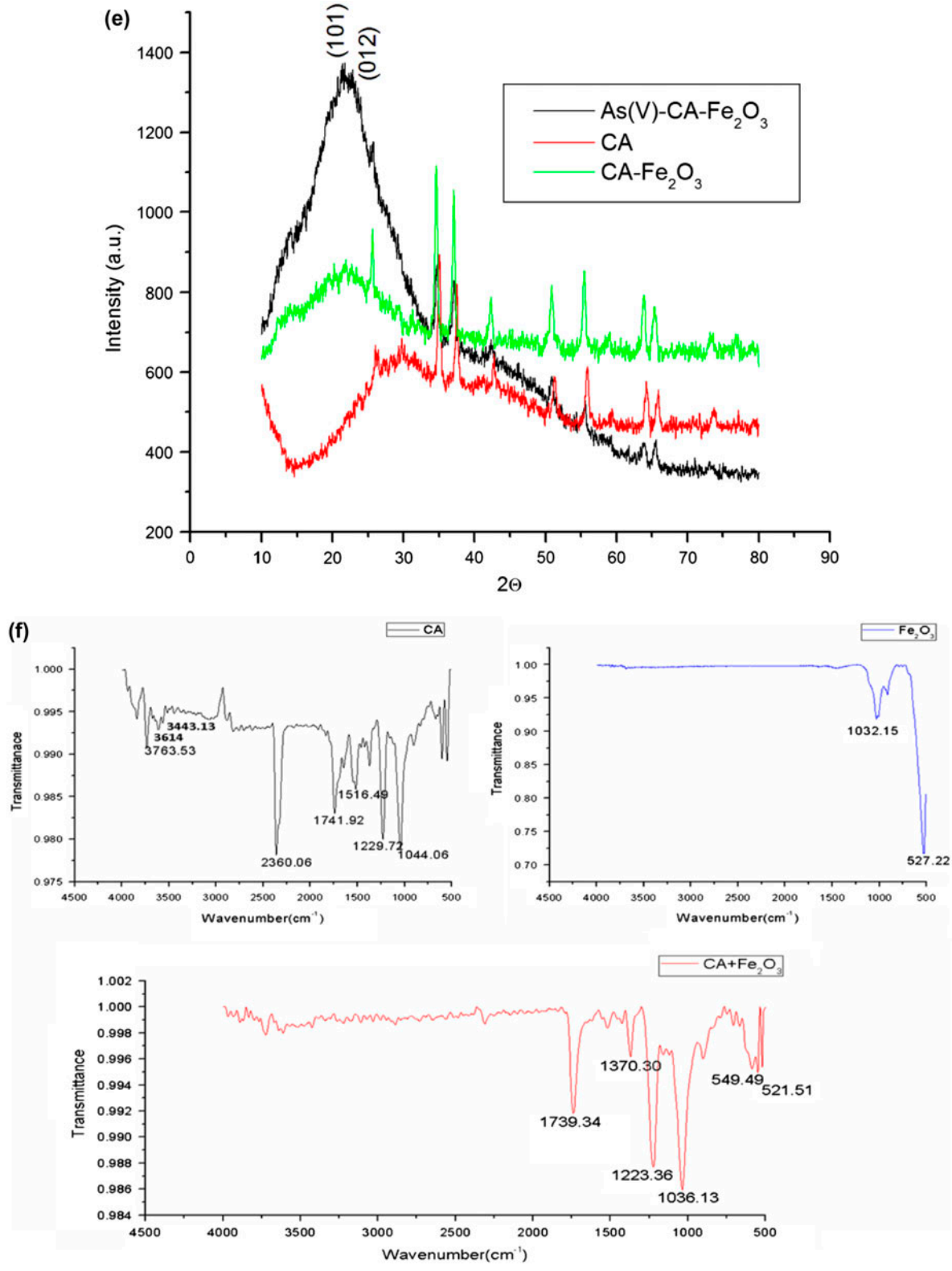


Fig. 3. (*Continued*).

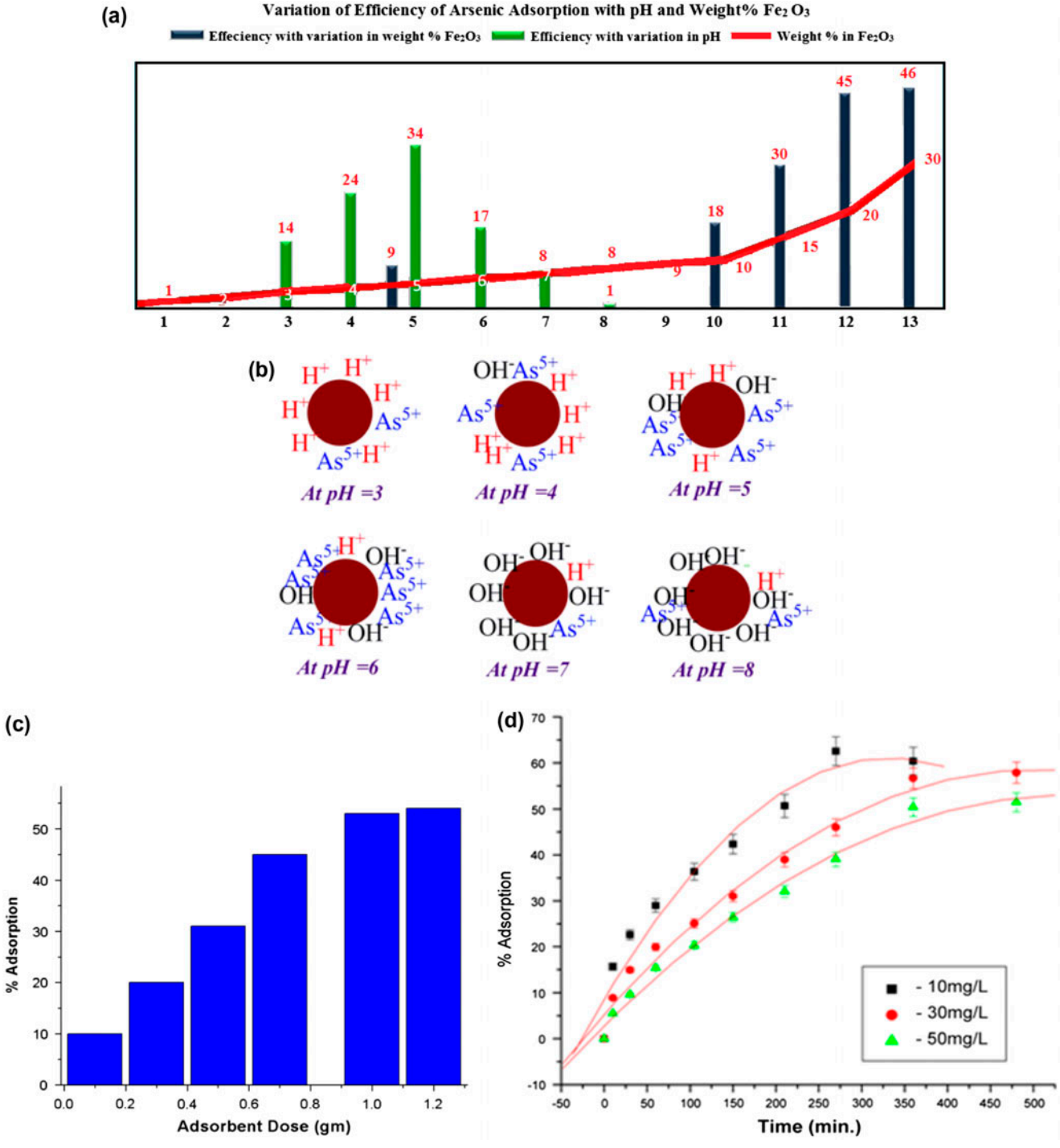


Fig. 4. (a) Effect of pH and weight % $Fe_2O_3$ loading in the beads on adsorption of As (V) ions, (b) Schematic depicting the configuration of ions around pH at different pH, (c) Effect of dose of the adsorbent on adsorption of As (V) ions, and (d) Effect of contact time and initial concentration of As (V) ions in solution on the adsorption of As (V) ions onto the beads.

selected as optimum pH throughout the research. The optimized pH is maintained throughout the process using the acid and bases.

#### 3.2.2. Influence of weight % $Fe_2O_3$ loading on adsorption

$Fe_2O_3$ weight % was varied from 1 to 30% in cellulose beads to analyse the adsorption behavior under optimized conditions (pH 5, adsorbent dose 1gm, As (V) concentration 10 mg $L^{-1}$, and contact time 240 min). Significant increase in adsorption was observed up to 20 wt.% $Fe_2O_3$ loading (Fig. 4(a)). However, with further increment in wt.%, the extent of increase in adsorption was minimal and remained almost consistent. Hence, 20 wt.% $Fe_2O_3$ loading was considered to be optimum condition. At higher weight % $Fe_2O_3$, the homogeneity of the dispersion of $Fe_2O_3$ in the polymer matrix was poor due to which the extent of adsorption of As (V) ions onto the beads did not increase.

#### 3.2.3. Effect of sorbent amount on adsorption

The adsorption efficiency was recorded with varying sorbent dose under optimized conditions. (pH 5, 20 wt.% $Fe_2O_3$, 10 mg/L As (V) concentration, and contact time 240 min.) Adsorption percentage was found to remarkably increased with sorbent amount due to greater availability of the active sites or surface area available on the adsorbent [36]. At optimum dose of beads, 100 mg in this case, 55% of adsorption was recorded. With further increase in dosage amount, there was no significant variation in adsorption primarily due to instauration of active sites [37]. Fig. 4(c) represents the variation of percentage adsorption of As (V) ions with variance in dose (weight of beads).

#### 3.2.4. Influence of initial As (V) ion concentration

The adsorption behavior of As (V) ions on hybrid cellulose beads was studied with varying initial As (V) ion concentration from 10 to 50 mg $L^{-1}$ while keeping all other parameters constant. (pH 5, 1gm adsorbent dose, 20% weight $Fe_2O_3$, and contact time 240 min.) Rise in adsorption capacity was observed while, adsorption efficiency was found to depreciate with increasing initial As (V) ion concentration (Fig. 4(d)). Increase in adsorption capacity was observed with increasing As (V) ion concentration, since it provides a driving force to overcome all mass transfer hindrances of metal ions between the aqueous and solid phase [38]. However, the sorption efficiency decreases due to limited availability of active sites.

#### 3.2.5. Time dependent adsorption

The plot of adsorption of As (V) ions as a function of time is depicted in Fig. 4(d). It revealed that the extent of As (V) ions removal increased with increasing contact time till equilibrium was attained. The elimination of As (V) ions by adsorption onto the beads was rapid for initial span and slowed down as the contact time increased till the system achieved equilibrium. This was caused by the initial instantaneous adsorption of As (V) ions on the external surface of the beads due to boundary layer diffusion followed by controlled pore diffusion into the intraparticle matrix leading to equilibrium [39].

### 3.3. Equilibrium adsorption isotherms

The equilibrium adsorption isotherms indicate the adsorption mechanism, surface properties and distribution of analyte ions between the liquid and the solid phase at equilibrium. Collection of sorption data at different As (V) concentration was analysed by fitting it into various well-known isotherm models like Langmuir, Freundlich, Temkin, and D–R [40].

#### 3.3.1. Langmuir isotherm model

Langmuir presented a model which assumes the formation of a monomolecular layer, on a homogenous surface without any interaction between the adsorbed molecules. The energy of adsorption remains constant throughout the process. Maximum capacity of the adsorbent can be predicted using Langmuir adsorption isotherm is given by Eq. (4):

$$q_e = (q_{max} K_L C_e)/(1 + K_L C_e) \quad (4)$$

where $C_e$ is the equilibrium concentration of As (V) ions (mg $L^{-1}$), $q_e$ is the amount of As (V) ions adsorbed at equilibrium (mg/g), $q_{max}$ is the maximum adsorption capacity of the adsorbent for a complete monolayer (mg $g^{-1}$), and $K_L$ is Langmuir adsorption constant which is a function of free energy of adsorption (L $mg^{-1}$). The linearized equation for Langmuir model is given as:

$$C_e/q_e = (1/q_{max} K_L) + (C_e/\ q_{max}) \quad (5)$$

The values of $q_{max}$ and $K_L$ are calculated from the slope and intercept of the straight line obtained by plotting $C_e/q_e$ vs. $C_e$ as shown in Fig. 5(a). To investigate the progression of adsorption process, a

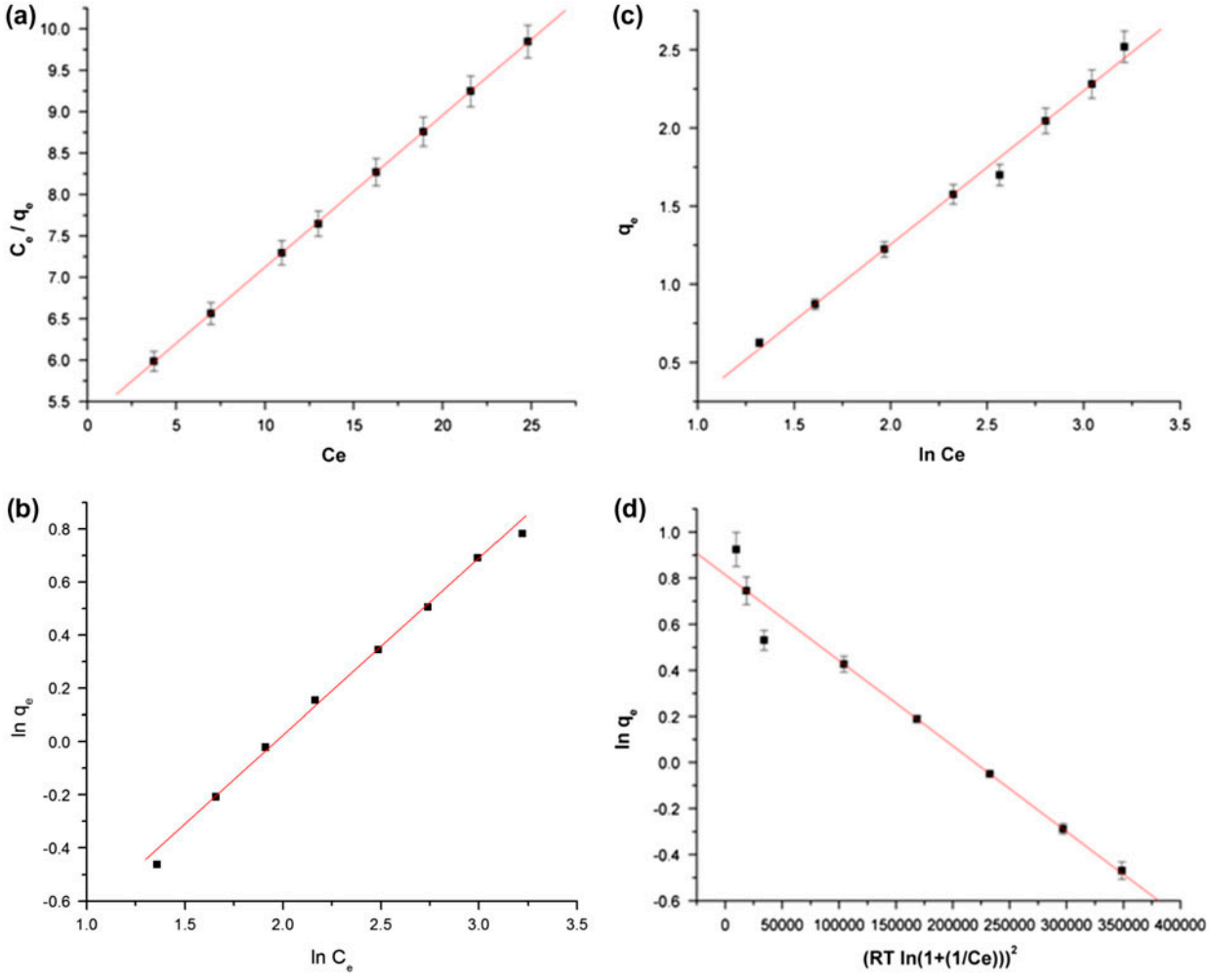


Fig. 5. Equilibrium adsorption isotherm models (a) Langmuir adsorption isotherm, (b) Freundlich adsorption isotherm, (c) Temkin adsoprtion isotherm, and (d) D–R adsorption isotherm.

dimensionless equilibrium constant referred to as separation factor, $R_L$ for Langmuir isotherm is calculated using Eq. (6):

$$R_L = 1/(1 + K_L C_0) \quad (6)$$

where $K_L$ (L mg$^{-1}$) is the Langmuir adsorption constant and $C_0$ (mg L$^{-1}$) is the initial concentration of analyte ions. The value of $R_L$ gives the interpretation about whether the adsorption is irreversible ($R_L = 0$), favorable ($0 < R_L < 1$), linear ($R_L = 1$), or unfavorable ($R_L > 1$).Determined value of the dimensionless factor $R_L$ is 0.53, indicating favorable adsorption of As (V) ions onto the adsorbent.

### 3.3.2. Freundlich Isotherm model

The Freundlich isotherm model considers that adsorption process occurs on heterogeneous surfaces and relates the concentration of analyte ions at equilibrium to the adsorption capacity [41]. This model is applicable to monolayer chemisorption as well as multilayer physisorption processes. This model is defined by the equation:

$$q_e = (K_F C_e)^{\frac{1}{n}} \quad (7)$$

where $q_e$ and $C_e$ are the equilibrium concentrations of As (V) ions adsorbed on solid (mg/g) and in the liquid phase (mg/L), respectively. $K_F$ and $n$ are the

Freundlich constants related to adsorption capacity and adsorption intensity, respectively. Equation in linearized form is given as [41,42]:

$$\ln q_e = (1/n)\ (\ln C_e) + \ln K_F \quad (8)$$

The value of constants $n$ and $K_F$ are obtained from slope and intercept of plot (Fig. 5(b)) between log $q_e$ vs. log $C_e$, respectively. The value of $n > 1$ indicates favorable adsorption. Larger value of $n$ (1–10) indicates strong interactions between adsorbent and adsorbate. The value of $n$ obtained for hybrid magnetized beads is 1.34, indicating favorable chemical interactions between the adsorbent and analyte ions.

### 3.3.3. Temkin isotherm model

Temkin isotherm model states that the adsorption process is uniformly distributed and the fall in heat of adsorption is linear with coverage and adsorbate–adsorbent interactions [43], and not logarithmic, as stated in the Freundlich model. Temkin isotherm is described by Eq. (9) [44] as:

$$q_e = [(RT/b_T)\ln(a_T C_e)] + (RT/b_T)\ln C_e \quad (9)$$

where $R$ is gas constant 8.314 J mol$^{-1}$ K$^{-1}$, $T$ is absolute temperature (K), $b_T$ is the Temkin constant related to the heat of adsorption (J mol$^{-1}$), and $a_T$ is the Temkin isotherm constant corresponding to the maximum binding capacity (L g$^{-1}$) [45–47]. The graph (Fig. 5(c)) between $q_e$ vs. ln $C_e$ is plotted to calculate the constants $b_T$ and $a_T$ from its slope and intercept, respectively. Values of constants, as shown in Table 1, suggest that adsorption follows this model to a certain extent with a convincing linear fit data.

### 3.3.4. D–R isotherm model

D–R isotherm model estimates the mean free energy of adsorption. It also considers the effect of porosity of the adsorbent on adsorption. The D–R isotherm is given by the following equation [48]:

$$\ln q_e = \ln q_{max} - K\varepsilon^2 \quad (10)$$

where $K$ (mol$^2$ J$^{-2}$) is D–R isotherm constant related to the mean adsorption energy. $q_{max}$ is the maximum adsorption capacity of complete monolayer (mg g$^{-1}$), $q_e$ is the amount of As (V) ions adsorbed per unit weight of the adsorbent at equilibrium(mg g$^{-1}$), and $\varepsilon$ is Polanyi potential and is estimated by:

$$\varepsilon = RT \ln [1 + (1/C_e)] \quad (11)$$

where $R$ is the gas constant (J mol$^{-1}$ K$^{-1}$) and $T$ is the absolute temperature (K). The slope of the plot ln $q_e$ vs. $\varepsilon^2$ gives the value of the constant K and $q_{max}$ is obtained from the intercept. Fig. 5(d) depicts the plot of D–R model yielding high correlation coefficient value.

The above results indicate that the Langmuir, Freundlich, and Temkin equilibrium adsorption isotherm models fit well for the adsorbate–adsorbent system. It is predicted that the initial monolayer adsorption occurs (which is confirmed from Langmuir model) leading to further multilayered chemical interactions between the As (V) ions and the beads as explained by the Freundlich isotherm. The Temkin

Table 1
Demonstration of equilibrium adsorption isotherm parameters

| Adsorption isotherm | Isotherm parameters | Values of parameters for As (V) ion |
|---|---|---|
| Langmuir | $q_{max}$ (mg g$^{-1}$) | 5.45 |
| | $K_L$ (L mg$^{-1}$) | 0.035 |
| | $R_L$ | 0.53 |
| | $R^2$ | 0.9998 |
| Freundlich | $n$ | 1.34 |
| | $K_F$ (mg g$^{-1}$) | 0.24 |
| | $R^2$ | 0.9958 |
| Temkin | $b_T$ (J mol$^{-1}$) | 2,537.70 |
| | $a_T$ (Lg$^{-1}$) | 0.49 |
| | $R^2$ | 0.9894 |
| (D–R) | $q_{max}$ (mg g$^{-1}$) | 2.26 |
| | $K \times 10^{-6}$ (mol$^2$ J$^{-2}$) | −3.7 |
| | $R^2$ | 0.9127 |
| | $\varepsilon$ | 291.28 |

isotherm explains that the process of adsorption is physico-chemical involving the hydroxyl (–OH) groups of the adsorbent system and the effect of porosity of the adsorbent on the process of adsorption is explained by the D–R isotherm model. The values of different equilibrium isotherm parameters calculated on the basis of these models are listed in Table 1.

### 3.4. Adsorption kinetics

Adsorption kinetics has been thoroughly studied to investigate the mechanism of adsorption and potential rate controlling steps in the whole process. The kinetic parameters are essential for the determination of adsorption rate and give vital information for designing and modeling the batch system. Several kinetic models (pseudo-first-order, pseudo-second-order, Elovich model, and intraparticle diffusion model) have been exploited to define the rate determining step and mechanism of adsorption to select optimum conditions for large scale applications [46].

#### 3.4.1. Pseudo-first-order model

Lagergren pseudo-first-order model demonstrates that the rate of adsorption of solute onto the adsorbent depends on the adsorption capacity. The pseudo-first-order rate equation is used to estimate the $k_{ad}$, the mass transfer coefficient. This model is used to describe the kinetics of solid–liquid phase adsorption. The pseudo-first-order rate equation is given as [38,49]:

$$dq/dt = k_1(q_e - q_t) \quad (12)$$

The above equation is integrated with boundary conditions, $q_t = 0$ at $t = 0$ and $q_t = q_e$ at $t = t$ and rearranged to get,

$$\log(q_e - q_t) = \log q_e - (k_1/2.303)t \quad (13)$$

where $q_e$ and $q_t$ are the amounts of adsorbed As (V) ions onto the adsorbent (mg/g) at equilibrium and at time $t$, respectively, and $k_1$ is the pseudo-first-order adsorption rate constant ($min^{-1}$). A straight line with a negative slope for the graph of log ($q_e$–$q_t$) vs. time suggests the applicability of pseudo-first-order kinetic model as evident from Fig. 6(a). A higher $R^2$ value indicates good fit of this model to the adsorption As (V) ions on to $Fe_2O_3$-loaded beads.

#### 3.4.2. Pseudo-second-order model

The pseudo-second-order kinetic model considers that rate of adsorption is directly proportional to the number of active sites present on the adsorbent surface [50]. It is also influenced by amount of adsorbate adsorbed onto the surface of the adsorbent at time $t$ and at equilibrium. This model can be applied over a whole range of data to predict the adsorption kinetics. This model assumes chemisorption as the rate-limiting step in the adsorption process. The pseudo-second-order equation is given as [36,49,51] given by Eq. (14):

$$dq/dt = k_{p2}(q_e - q_t)^2 \quad (14)$$

After rearranging and integrating the above equation with boundary conditions, $q_t = 0$ at $t = 0$ and $q_t = q_e$ at $t = t$, following Eq. (15) is obtained:

$$t/q_t = (1/k_2 q_e) + (t/q_e) \quad (15)$$

where $k_2$ (g/mg min) is the pseudo-second-order rate constant, $q_t$ and $q_e$ are the amount of As (V) ions adsorbed onto the surface of the adsorbent at time $t$ and at equilibrium, respectively (mg/g).

#### 3.4.3. Elovich model

Chemisorption processes are described by means of Elovich model. Elovich equation is based on the adsorption capacity describing the kinetics of chemisorption on highly heterogeneous adsorbent surface and is expressed as:

$$dq_t/dt = \alpha e_t^{-\beta q} \quad (16)$$

where $q_t$ (mg $g^{-1}$) is the amount of As (V) ions adsorbed at time $t$, $\beta$ is the desorption constant related to extent of surface coverage and activation energy of the chemisorption, and $\alpha$ is the initial adsorption rate. After rearranging and integrating the above equation with boundary conditions, $q_t = 0$ at $t = 0$, and $q_t = q_t$ at $t = t$ assuming $\alpha\beta >> t$ is given as:

$$q_t = (\ln \alpha\beta/\beta) + (\ln t/\beta) \quad (17)$$

This linearized form of Elovich kinetic equation yields a plot of $q_t$ vs. ln $t$, which gives a straight line as seen in Fig. 6(c), indicating good correlation between the experimental data and theoretical model. High value

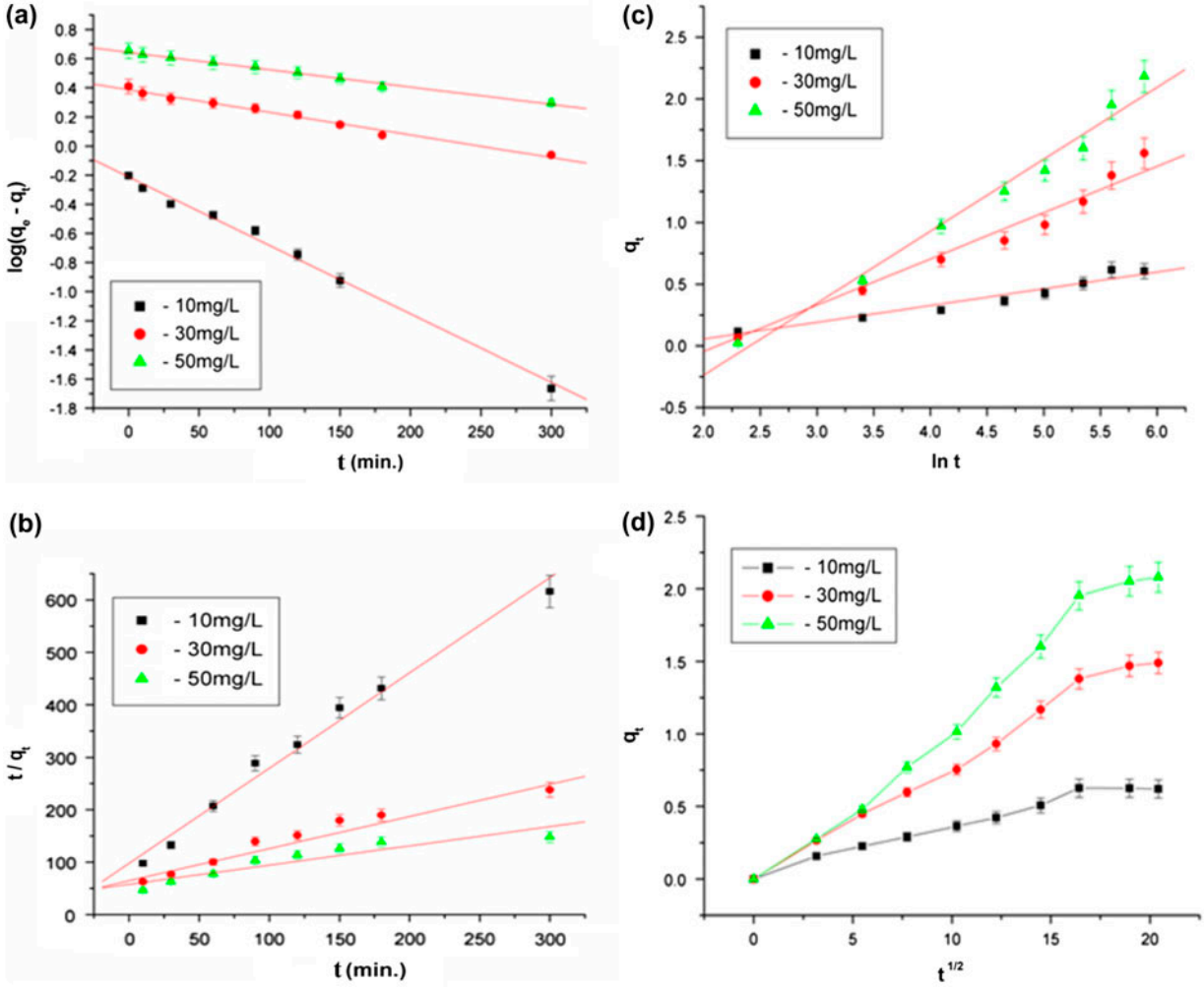


Fig. 6. Kinetic models (a) Pseudo-first-order kinetic model, (b) Pseudo-second-order kinetic model, (c) Elovich kinetic model, and (d) Intraparticle diffusion kinetic model.

of regression coefficients ($R^2$) at all concentrations suggests propinquity of the adsorbance reactions to Elovich model.

### 3.4.4. Intraparticle diffusion model

The rate-limiting step, which is governed by adsorption mechanism, is a significant factor in determining the mechanism of the adsorption process. Intraparticle diffusion model is used to determine the adsorption mechanism of analyte ions onto impregnated cellulose beads. For a solid–liquid adsorption process, the solute transfer usually occurs by external mass transfer (boundary layer diffusion), intraparticle diffusion (pore diffusion), or both. According to Weber and Morris, the intraparticle diffusion coefficient $k_{int}$ is given by the equation [52]:

$$q_t = K_{int} t^{0.5} + I \quad (18)$$

where $k_{int}$ is the intraparticle diffusion rate constant (mg/ g $min^{0.5}$) and $I$ is the intercept. The plot of $q_t$ vs. $t^{0.5}$ (Fig. 6(d)) does not pass through the origin and shows multilinearity indicating the occurrence of multiple steps in adsorption process [28]. Boundary layer diffusion accounts for the instantaneous adsorption of As (V) ions on the external surface of the beads, which is reflected by first sharper portion of the plot. Value of I indicates thickness of the boundary layer (Table 2). The second portion is the gradual adsorption stage with controlled pore diffusion, where As (V) ions move into the interior of the beads. The third step indicates the attainment of equilibrium stage, where intraparticle diffusion starts to slow down due to severely low concentration of adsorbate

Table 2
Demonstration of adsorption kinetic parameters

| Kinetic model | Concentration | 10 mg $L^{-1}$ | 30 mg $L^{-1}$ | 50 mg $L^{-1}$ |
|---|---|---|---|---|
| Pseudo-first-order Model | $k_1$ ($min^{-1}$) | −0.01082 | −0.00357 | −0.00274 |
| | $R^2$ | 0.9874 | 0.9858 | 0.9922 |
| Pseudo-second-order model | $k_2$ (g $mg^{-1}$ $min^{-1}$) | 0.3379 | 0.0577 | 0.0232 |
| | $R^2$ | 0.9551 | 0.8337 | 0.7949 |
| Elovich model | $\alpha$ (mg $g^{-1}$ $min^{-1}$) | 0.14 | 0.37 | 0.58 |
| | $\beta$ | 1.51 | 0.32 | 0.15 |
| | $R^2$ | 0.9133 | 0.8721 | 0.8632 |
| Intraparticle diffusion model | $k_{int}$ (mg $g^{-1}$ $min^{-0.5}$) | 0.033 | 0.086 | 0.13 |
| | L | 0.032 | −0.043 | −0.17 |

in the solution. The intraparticle diffusion rate is obtained from the slope of the gentle-sloped portion of the graph. The results suggests that the adsorption data of As (V) ions from aqueous solution using the magnetized cellulose acetate beads gives satisfactory fit for pseudo-first order, Elovich, and Intraparticle diffusion models. High value of regression coefficient ($R^2$) for these kinetic models suggests that the adsorption of As (V) ions onto the beads can be well explained by these models. The applicability of Elovich model predicts the involvement of chemisorption. The multilinear graphs obtained for the Intraparticle diffusion model confirms that initially there will be an instantaneous adsorption of As (V) ions onto the surface of the adsorbent system through film or surface diffusion. After sometime when the surface coverage increases there will be gradual adsorption through controlled intraparticle or pore diffusion, where As (V) ions move into the interior of the beads and at a later stage, when the equilibrium is attained the intraparticle diffusion begins to slow down. Table 2 represents the parameters calculated from different kinetic models.

### 3.5. Desorption experiments

Reusability of adsorbent and recovery of As (V) ions, desorption experiments were conducted with a series of varied reagents viz, formic acid, acetic acid, hydrochloric acid, ammonium hydroxide, and sodium hydroxide [24,30]. Among the various reagents used, 0.1 M $CH_3COOH$ and 0.1 M HCOOH effectively recover the As (V) ions at pH 5.0 adsorbed by adsorbent. As (V) ions of 91 and 94% were recovered using 0.1 M $CH_3COOH$ and HCOOH due to displacement of $H^+$ by As (V) ion and formation of stable complexes. The experimental results (Fig. 7) revealed that desorption percentage increases from 59 to 94% within 30 min, thereafter, equilibrium is achieved i.e. no change in desorption yield [38]. Therefore, As (V) ions could be desorbed successfully using 0.1 M $CH_3COOH$ and HCOOH, and effectively used for the regeneration of the adsorbent. Several experiments were performed and the study suggest that the system is reused for five adsorption-desorption cycles.

### 3.6. Adsorption thermodynamics

The thermodynamic parameter, Gibb's free energy change ($\Delta G$) is essential to know the spontaneity of the adsorption process [53]. At a given temperature, if the value of ($\Delta G$) is negative then the reaction is spontaneous. The adsorption of As (V) ions onto cellulose beads loaded with ferric oxide was studied at a temperature of 300 K. The free energy of adsorption ($\Delta G$) was calculated from Eq. (19):

$$\Delta G = -RT \ln K_L \quad (19)$$

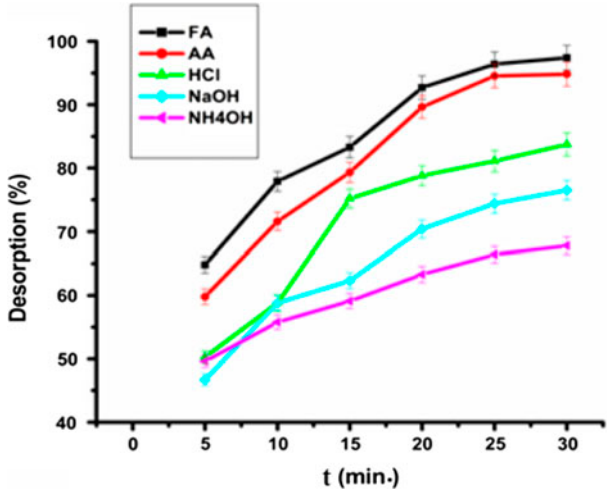


Fig. 7. Effect of contact time on % desorption of As (V) ions.

where $K_L$ is Langmuir isotherm constant, $R$ is universal gas constant (8.314 J/mol K), and $T$ is absolute temperature (K). The change in free energy ($\Delta G$) value obtained for uptake of As (V) ions is −8.38 kJ/mol. The negative value of $\Delta G$ establishes the feasibility and spontaneity of the adsorption process.

## 4. Conclusions

The present prospective deals with the preparation of cellulose acetate beads impregnated with $Fe_2O_3$ by precipitation polymerization technique and utilize it for the expunging of As (V) ions from the mimicked solution. Batch adsorption experiments were executed for elimination of As (V) ions, using 1 gm of adsorbent dosage, under optimized conditions, the experimental data were analysed using the kinetics and adsorption isotherm models. The results depicts that, the $Fe_2O_3$ functionalized cellulose acetate beads could remove 65% of As (V) ions effectively in 4 h. Based on the regression coefficient values, Langmuir isotherm model is in commendable agreement to describe the adsorption process. Thus, the adsorption was found to obey monolayer formation further proceeding to multilayer adsorption of analyte ions. The kinetic studies indicate that sorption followed pseudo-first-order model, thermodynamics parameters revealed, the process is a highly spontaneous and feasible adsorption reaction. The specific surface area of the sorbent was computed using the BET analysis; XRD was used to investigate the phase structure of magnetised cellulose acetate beads prior to and after the adsorption of As (V) ions. FTIR was performed to examine the interactions between acetate and hydroxyl groups of cellulose acetate and iron. The $Fe_2O_3$ incorporated cellulose acetate beads stable up to five effective adsorption-desorption cycles, thereafter, 5% decrease in the adsorption efficiency was recorded in the desorption experiment performed using various acid bases. The present study suggests that, due to the cost-effectiveness, environment suitability and efficiency of removal of As (V) ions from the mimicked solution within 4 h, the proposed adsorbent can be produced on large scale to removal of As (V) from industrial effluents.

## Acknowledgments

Authors thank Dr Surendra K. Pal, Vice Chancellor, DIAT (DU) for the encouragement and support and DIAT-DRDO Nano Project Program (EPIPR/1003883/M/01/908/2012/D (R&D)/1416 Dated: 28.03.2012, DRDO HQ, New Delhi) for financial assistance. The authors express their sincere gratitude towards Dr Robin McIntyre, Iconiq Innovations, for English language and spelling corrections. Also, would like to thank Jyothi D. Mumbrekar and Dr Renuka Gonte for technical assistance.

## References

[1] H. Garelick, H. Jones, A. Dybowska, E.V. Jones, Arsenic pollution sources, Rev. Environ. Contam. Toxicol. 197 (2008) 17–60.
[2] A. Pillai, G. Sunita, V.K. Gupta, A new system for the spectrophotometric determination of arsenic in environmental and biological samples, Anal. Chim. Acta 408 (2000) 111–115.
[3] B.M. Jovanović, V.L. Vukašinović-pešić, Đ.N. Veljović, L.V. Rajaković, Arsenic removal from water using low-cost adsorbents: A comparative study, J. Serb. Chem. Soc. 76 (2011) 1437–1452.
[4] H. Guo, D. Stüben, Z. Berner, Adsorption of arsenic (III) and arsenic (V) from groundwater using natural siderite as the adsorbent, J. Colloid Interface Sci. 315 (2007) 47–53.
[5] D. Mohan, C.U. Pittman Jr, Arsenic removal from water/wastewater using adsorbents—A critical review, J. Hazard. Mater. 142 (2007) 1–53.
[6] S.V. Flanagan, R.B. Johnston, Y. Zheng, Arsenic in tube well water in Bangladesh: Health and economic impacts and implications for arsenic mitigation, Bull. World Health Organ. 90 (2012) 839–846.
[7] Environmental Fact Sheet, Arsenic in Drinking Water, 2003, WD-WSEB-3-2, Available from: <www.centralsupplyinc.com/statenh/ws-3-2.htm>.
[8] J.F. Ferguson, J. Gavis, A review of the arsenic cycle in natural waters, Water Res. 6 (1972) 1259–1274.
[9] A. Tiwari, T. Dewangan, A.K. Bajpai, Removal of toxic As (V) ions by adsorption onto alginate and carboxymethyl cellulose beads, J. Chin. Chem. Soc. 55 (2008) 952–961.
[10] L. Dupont, G. Jolly, M. Aplincourt, Arsenic adsorption on lignocellulosic substrate loaded with ferric ion, Environ. Chem. Lett. 5 (2007) 125–129.
[11] P.K. Pandey, S. Choubey, Y. Verma, M. Pandey, K. Chandrashekhar, Biosorptive removal of arsenic from drinking water, Bioresour. Technol. 100 (2009) 634–637.
[12] K.S. Prasad, P. Srivastava, V. Subramanian, J. Paul, Biosorption of As (III) ion on *Rhodococcus* sp. biomass characterization and kinetic studies, Sep. Sci Technol. 46 (2011) 2517–2525.
[13] Y. Ku, I.L. Jung, Photocatalytic reduction of Cr (VI) in aqueous solutions by UV irradiation with the presence of titanium dioxide, Water Res. 35 (2001) 135–142.
[14] L. Makhloufi, B. Saidani, H. Hammache, Removal of lead ions from acidic aqueous solutions by cementation on iron, Water Res. 34 (2000) 2517–2524.
[15] A. Smara, R. Delimi, E. Chainet, J. Sandeaux, Removal of heavy metals from diluted mixtures by a hybrid ion-exchange/electrodialysis process, Sep. Purif. Technol. 57 (2007) 103–110.
[16] B. Alyüz, S. Veli, Kinetics and equilibrium studies for the removal of nickel and zinc from aqueous solution by ion exchange resins, J. Hazard. Mater. 167 (2009) 482–488.

[17] K. Seong Ng, Z. Ujang, P. Le-Clech, Arsenic removal technologies for drinking water treatment, Rev. Environ. Sci. Biotechnol. 3 (2004) 43–53.
[18] W. Ying, Z. Kongjun, W. Fen, Y. Kazumichi, Novel Fe/glass composite adsorbent for As (V) removal, J. Environ. Sci. 21 (2009) 434–439.
[19] V. Kumar, N. Talreja, D. Deva, N. Sankararamakrishnan, A. Sharma, N. Verma, Development of bi-metal doped micro- and nano multi-functional polymeric adsorbents for the removal of fluoride and arsenic (V) from wastewater, Desalination 282 (2011) 27–38.
[20] X. Guo, F. Chen, Removal of arsenic by bead cellulose loaded with iron oxyhydroxide from groundwater, Environ. Sci. Technol. 39 (2005) 6808–6818.
[21] M. Valcárcel, B.M. Simonet, S. Cárdenas, B. Suárez, Present and future applications of carbon nanotubes to analytical science, Anal. Bioanal. Chem. 382 (2005) 1783–1790.
[22] N. Tavakkoli, S. Habibollahi, S.A. Tehrani, Separation and preconcentration of arsenic (III) ions from aqueous media by adsorption on MWCNTs, Arabian J. Chem. (2014) (accepted manuscript) doi: 10.1016/j.arabjc.2014.04.007.
[23] Y.F. Lin, J.L. Chen, Magnetic mesoporous Fe/carbon aerogel structures with enhanced arsenic removal efficiency, J. Colloid Interface Sci. 420 (2014) 74–79.
[24] P. Rule, K. Balasubramanian, R.R. Gonte, Uranium (VI) remediation from aqueous environment using impregnated cellulose beads, J. Environ. Radioact. 136 (2014) 22–29.
[25] M. Urík, P. Littera, J. Ševc, M. Kolenčík, S. Čerňanský, Removal of arsenic (V) from aqueous solutions using chemically modified sawdust of spruce (*Piceaabies*): Kinetics and isotherm studies, Int. J. Environ. Sci. Technol. 6(3) (2009) 451–456.
[26] C.S. Rao, S.C. Rajan, N.V. Rao, Spectrophotometric determination of arsenic by molybdenum blue method in zinc-lead concentrates and related smelter products after chloroform extraction of iodide complex, Talanta 40 (1993) 653–656.
[27] T. Cherian, B. Narayana, A new spectrophotometric method for the determination of arsenic in environmental and biological samples, Anal. Lett. 38 (2005) 2207–2216.
[28] X. Cao, R. Prozorov, Y. Koltypin, G. Kataby, I. Felner, A. Gedanken, Synthesis of pure amorphous $Fe_2O_3$, J. Mater. Res. 12 (1996) 402.
[29] H. Kamal, F.M.A. Abd-Elrahim, S. Lotfy, Characterization and some properties of cellulose acetate-co-polyethylene oxide blends prepared by the use of gamma irradiation, J. Radiat. Res. Appl. Sci. 7(2) (2014) 146–153.
[30] N. Singh, K. Balasubramanian, An effective technique for removal and recovery of Uranium (VI) from aqueous solution using cellulose-camphor soot nanofibers, RSC Adv. 4(2014) 27691–27701.
[31] B.N. Sahoo, K. Balasubramanian, Photoluminescent carbon soot particles derived from controlled combustion of camphor for superhydrophobic applications, RSC Adv. 4 (2014) 11331–11342.
[32] B. Bock, K. Flatau, H. Junge, M. Kuhr, H. Musso, Bond character of beta di-ketone metal chelates, Angew. Chem. Int. Ed. 10(4) (2003) 225–235.
[33] G.H. Spikes, E. Bill, T.W. Weyhermüller, K. Wieghardt, Transition-metal complexes with singly reduced 1,2-diketone radical ligands, Angew. Chem. 120 (2008) 3015–3019.
[34] A. Kongdee, T. Bechtold, Influence of ligand type and solution pH on heavy metal ion complexation in cellulosic fibre: Model calculations and experimental results, Cellulose 16 (2009) 53–63.
[35] S.T. Sundar, M.M. Sain, K. Oksman, Characterization of microcrystalline cellulose and cellulose long fiber modified by iron salt, Carbohydr. Polym. 80 (2010) 35–43.
[36] O. Abdelwahab, Kinetic and isotherm studies of copper (II) removal from wastewater using various adsorbents, Egypt. J. Aquat. Res. 33 (2007) 125–143.
[37] A. Shukla, Y.H. Zhang, P. Dubey, J.L. Margrave, S.S. Shukla, The role of sawdust in the removal of unwanted materials from water, J. Hazard. Mater. 95 (1–2) (2002) 137–152.
[38] R.R. Gonte, G. Shelar, K, Balasubramanian. Polymer–agro-waste composites for removal of Congo red dye from wastewater: Adsorption isotherms and kinetics, Desalin. Water Treat. (2013) 7797–7811, doi: 10.1080/19443994.2013.833876.
[39] O. Hamdaoui, M. Chiha, Removal of methylene blue from aqueous solutions by wheat bran, Acta Chim. Slov. 54 (2007) 407–418.
[40] T.S. Anirudhan, P.S. Suchithra, P. Senan, A.R. Tharun, Kinetic and equilibrium profiles of adsorptive recovery of thorium (IV) from aqueous solutions using poly (methacrylic acid) grafted cellulose/bentonite superabsorbent composite, Ind. Eng. Chem. Res. 51 (2012) 4825–4836.
[41] A. Benhamou, M. Baudu, Z. Derriche, J.P. Basly, Aqueous heavy metal removal on amine functionalized Si-MCM-41 and Si-MCM-48, J. Hazard. Mat. 171 (2009) 1001–1008.
[42] H. Zheng, D. Liu, Y. Zheng, S. Liang, Z. Liu, Sorption isotherm and kinetic modeling of aniline on Cr-bentonite, J. Hazard. Mater. 167 (2009) 141–147.
[43] G.D. Halsey, The role of surface heterogeneity in adsorption, Adv. Catal. 4 (1952) 259–269.
[44] T.M. Elmorsi, Equilibrium isotherms and kinetic studies of removal of methylene blue dye by adsorption onto miswak leaves as a natural adsorbent, J. Environ. Prot. 02(06) (2011) 817–827.
[45] M. Kumar, Y. Ando, Controlling the diameter distribution of carbon nanotubes grown from camphor on a zeolite support, Carbon 43 (2005) 533–540.
[46] Y. Liu, Y.J. Liu, Biosorption isotherms, kinetics and thermodynamics, J. Sep. Purif. Technol. 61 (2008) 229–242.
[47] A.K. Kaygun, S. Akyil, Study of the behavior of thorium adsorption on PAN-zeolite composite adsorbent, J. Hazard. Mater. 147 (2007) 357–362.
[48] B. Kiran, A. Kaushik, Chromium binding capacity of *Lyngbya putealis* exopolysaccharides, J. Biochem. Eng. 38(1) (2008) 47–54.
[49] H. Qiu, L. Lv, B.C. Pan, Q.J. Zhang, W.M. Zhang, Q.X. Zhang, Critical review in adsorption kinetic models, J. Zhejiang Univ. Sci. A 10 (2009) 716–724, doi: 10.1631/jzus.A0820524.

[50] Y.S. Ho, G. McKay, Pseudo-second-order model for sorption processes, Process Biochem. 34 (1999) 451–465.
[51] R.R. Gonte, K. Balasubramanian, Chemically modified polymer beads for sorption of gold from waste gold solution, J. Hazard. Mater. 217–218 (2012) 447–451.
[52] T.J. Sahetya, F. Dixit, K. Balasubramanian, Waste citrus fruit peels for removal of Hg (II) ions, Desalin. Water Treat. (2013) 1404–1416, doi: 10.1080/19443994.2013.852483.
[53] N.A. Oladoja, C.O. Aboluwoye, Y.B. Oladimeji, Kinetics and isotherm studies on methylene blue adsorption onto ground palm kernel coat, Turk. J. Eng. Environ. Sci. 32 (2008) 303–312.